Observation of *d*-wave Pomeranchuk nematic order in floating monolayer FeSe on FeSe/STO

X.-L. Peng[1,2*], K. Jiang[1*], Y.-H. Yuan[4], P. Zhang[5], G.-N. Phan[1], S.-Y. Gao[1,2], Y.-B. Huang[6], L.-Y. Kong[1], T. Qian[1,2,7], W. Li[4], Q.-K. Xue[4], Z.-Q. Wang[3], Y.-J. Sun[1,7,8†] & H. Ding[1,7,8†]

[1]*Beijing National Laboratory for Condensed Matter Physics, and Institute of Physics, Chinese Academy of Sciences, Beijing 100190, China*

[2]*School of Physics, University of Chinese Academy of Sciences, Beijing 100190, China*

[3]*Department of Physics, Boston College, Chestnut Hill, MA 02467, USA*

[4]*State Key Laboratory of Low-Dimensional Quantum Physics, Department of Physics, Tsinghua University, Beijing 100084, China*

[5]*Institute for Solid State Physics, University of Tokyo, Kashiwa, Chiba 277-8581, Japan*

[6]*Shanghai Advanced Research Institute, Chinese Academy of Sciences, Shanghai 201204, China*

[7]*Songshan Lake Materials Laboratory, Dongguan, Guangdong 523808, China*

[8]*CAS Center for Excellence in Topological Quantum Computation, University of Chinese Academy of Sciences, Beijing 100190, China*

[*] These authors contributed equally to this work

[†] Corresponding authors: yjsun@iphy.ac.cn; dingh@iphy.ac.cn

As a foundation of condensed matter physics, the normal states of most metals are successfully described by Landau Fermi liquid theory with quasi-particles and their Fermi surfaces (FSs). The FSs sometimes become deformed or gapped at low temperatures owing to quasi-particle interactions, known as FS instabilities. A notable example of a FS deformation that breaks only the rotation symmetry, namely Pomeranchuk instability, is the d-wave FS distortion, which is also proposed as one possible origin of electron nematicity in iron-based superconductors. However, no clear evidence has been made for its existence, mostly owing to the mixture of multiple orders. Here we report an unequivocally observation of the Pomeranchuk nematic order in floating monolayer (ML) FeSe on 1 ML-FeSe/SrTiO₃ substrate. By using angle-resolve photoemission spectroscopy, we find remarkably that the d_{xz} and d_{yz} bands are degenerate at the Brillouin zone center (Γ point), while their splitting is even larger at zone corner (M point), in stark contrast to that in bulk FeSe. Our detailed analysis show that the momentum-dependent nematic order in floating monolayer FeSe is coming from the d-wave Pomeranchuk instability at M point, shedding light on the origin of the ubiquitous nematicity in iron-based superconductors. Our results establish the single-layer high-T_c superconductors as an excellent material platform for investigating emergent quantum physics under complex intertwinement.

Electronic nematicity is defined as the breaking of the lattice rotational symmetry but preserving the translational symmetry in the electronic degrees of freedom. This phenomenon has attracted much attention for its ubiquity in strongly correlated systems, especially in copper oxide superconductors [1,2] and iron-based superconductors [3-6]. The origin of nematic order has been argued to be connected to the microscopic mechanism of unconventional superconductivity in iron-based superconductors [6,7,8], as reflected in their intimate relation revealed in the phase diagram. Phenomenologically, there are two types of nematic order in FeSe: Pomeranchuk instability induced FS distortion [8] and ferro-orbital order [9] owing to the occupation imbalance caused by the an isotropic lifting of the degeneracy of two atomic orbitals related by rotation symmetry. For Pomeranchuk instability

[10], the angular momentum $l=2$ quasiparticle interaction deforms the FS and leads to rotation symmetry breaking nematic order as shown in Fig.1a. Owing to crystal symmetry, the $l=2$ deformation corresponds to a d-wave ($cosk_x - cosk_y$) form factor, which indicates a vanishing nematic splitting gap at Γ point and maximum nematic gap at M point ($\Delta_\Gamma = 0$, $\Delta_M \neq 0$). On the other hand, the rotation symmetry always conserves the occupation degeneracy in symmetry related orbitals. For example, C_4 symmetry requires the charge density $n_{xz} = n_{yz}$ in FeSe. Therefore, a ferro-orbital order from the onsite energy difference, $\Delta_{FO}(d^+_{xz}d_{xz} - d^+_{yz}d_{yz})$, will induce a nematic order with homogeneous gaps ($\Delta_\Gamma = \Delta_M \neq 0$) as shown in Fig.1b. Since both of them belong to the same symmetry group, the two types of nematic order can appear simultaneously after the nematic transition. In recent ARPES studies, a sign-change momentum-dependent splitting gap ($\Delta_\Gamma \neq 0$, $\Delta_M \neq 0$ and $\Delta_\Gamma \times \Delta_M < 0$) was observed between the d_{xz} and d_{yz} orbitals in detwinned bulk materials [11-14], which indicates the coexistence of different nematic order parameters. However, the driving force remains controversial. In this work, we will show the nematic order of FeSe originates primarily from the d-wave Pomeranchuk instability induced FS distortion of the electron pockets at M point.

The nematic order emerges in FeSe thick films on SrTiO$_3$ (STO) when decreasing the temperature across the structural transition temperature T_{nem} [15,16]. As shown in Fig. 1c, stripes develop in the vicinity of impurities in the 20 monolayer (ML) FeSe films. The direction of the stripes changes 90° across the domain wall [16]. This change represents that the four-fold rotational symmetry in each domain is broken, which is direct evidence for electronic nematicity. Even when the film thickness decreases to 2 ML, the nematicity is still observed, as shown in Fig. 1d. However, stripes have not been reported in 1 ML FeSe/STO [17], which may be because the first layer of FeSe is strongly coupled to the STO substrate [18]. In contrast, the second layer of FeSe is so weakly coupled with the first layer that it can be evaporated by simply low-temperature annealing [19], like second layer of epitaxial grown graphene [20]. Therefore, the second layer could be regarded as the intrinsic monolayer floating on the 1 ML FeSe/STO [19,21,22]. The FS of 2 ML FeSe is shown in Fig. 1e, which

is consistent with previous results [19,23]. It should be noted that the hole-like bands around Γ point do not cross the Fermi level. The finite spectroscopic intensity observed around Γ is not from a FS but from the measurement resolution broadening, as shown in Fig. 1f and Fig. 2. Fig. 1f shows the band structure measured along the Γ - M direction. The hole-like band is below the Fermi energy (E_F), which indicates that the floating monolayer FeSe only contains FSs around the zone corner. The nematicity, which induces a splitting gap at the M point between the two hole-like bands, defined as Δ_M, is observed to be similar to the gap observed in the detwinned FeSe single crystal [12-14]. The gap size is ~70 meV, which is larger than that of ~50 meV detected in the bulk FeSe at T = 30 K [13]

In angle-resolved photoemission spectroscopy (ARPES) measurements, photons with different polarizations can excite electrons with different wave-function symmetries in crystals [24], and the definition of p- and s-polarization is given in our experimental geometry, as shown in Fig. 2a. The odd (even) orbital with respect to the M_x mirror plane can be observed with p- (s-) polarized photons. The band dispersion along the Γ - M direction measured by p-polarized photons is shown in Fig. 2b. Two hole-like bands α and β are clearly observed with different photon energies (hv = 26, 28, 32, and 42 eV, respectively). As the photon energy increases, the intensity of the α band decreases while that of the β band increases, which is due to the opposite photoemission cross sections of Fe $3d$ and Se $4p$ in the energy range of our experiments [25,26]. Therefore, we can conclude that the β band has the Fe d_{yz} orbital character and the α band contains part of the Se p_z orbital character. On the other hand, when the exciting photons are switched to s-polarization, only the α band is observed, as shown in Fig. 2e, confirming its d_{xz} orbital character.

Notably, unlike in bulk FeSe, the energy splitting between the α and β bands at the Γ point ($\Delta_Γ$) disappears, as shown in Fig. 2b(ii). To display the energy splitting more precisely, we plot the energy distribution curve (EDC) at the Γ point of data measured by 32 eV p- and s-polarized photons in Fig. 2d. We choose these two distinct exciting photons simply because these two different energy bands are enhanced by these photons, as shown in Fig. 2b(iii) and

Fig. 2e(iii). It is clearly shown that these two bands are degenerate. Moreover, to determine the band dispersion quantitatively, we extract the peak position of the momentum distribution curve (MDC) and use a parabola function to fit the data points, as shown in Fig. 2f. The fitting results of the band tops of the α and β bands are located at 9.39 ± 0.31 meV and 9.83 ± 1.05 meV below the Fermi energy (E_F), respectively. Again, this proves the nearly degenerate nature of the d_{xz} and d_{yz} bands at the Γ point. On general grounds, there are two common origins for the gap Δ_Γ at Γ point, the ferro-orbital order or spin-orbital coupling (SOC). However, these two cannot cancel each other since they are coupled to two different scattering channels. Therefore, the missing nematic gap of d_{xz} and d_{yz} bands at Γ point rules out the ferro-orbital order scenario. On the other hand, the large nematic gap around M point proves a *d*-wave nature of nematicity in floating monolayer FeSe, which is consistent with the Pomeranchuk instability induced FS distortion since the FSs only exist around M point.

To further investigate the evolution of the nematic order from an ultrathin film to bulk FeSe, we measured the band structure of 4, 20 and 60 ML FeSe films. Fig. 3 represents the Δ_Γ evolution as a function of the film thickness. As shown in Fig. 3a, the degeneracy of the two hole-like bands is lifted in 4 ML, and the band gap between them becomes larger as the film thickness increases. The gap value Δ_Γ, shown in Fig. 3b, increases gradually from 0 meV in 2 ML to 32 meV in 60 ML FeSe, which is similar to that in the bulk samples of FeSe [11,12,27]. This increase indicates that nematic splitting emerges in the multilayer film at the Γ point.

In Fig. 3c, by using 32 eV *p*- and *s*-polarized photons, we observe two sets of hole-like bands near the Γ point in 60 ML FeSe. It should be noted that there are twined nematic domains in the sample, so the two sets of energy bands belong to the d_{xz} and d_{yz} orbitals of different twin domains defined by their crystal coordinates, as shown in Fig. 3e(ii). In contrast, we only observe one set of energy bands of the 2 ML film in the same measurement, which is due to the absence of nematic order at Γ, as shown in Fig. 3e(i). Therefore, this observation is consistent with the *d*-wave nature of the nematicity in the 2 ML film. The band gaps (Δ_Γ) of

the 60 ML film measured by two different polarized photons show the same value, as shown in Fig. 3d.

To illustrate the band evolution more clearly, we summarize the binding energy of the d_{xz} and d_{yz} bands measured by 22 eV and 32 eV photons at the Γ point in Fig. 4a. In thick films, the binding energy of each band is changed when measured by different photon energies, which indicates the dispersion of the energy band along k_z in the thick film. Although the value of k_z is different, the nematicity-induced energy gaps are the same as those shown in Fig. 4b, where the results of Δ_Γ and Δ_M are presented as a function of thickness. As the thickness increases, Δ_Γ and Δ_M shift to positive values nearly in parallel, suggesting a mixture of the ferro-orbital order ($\Delta_\Gamma = \Delta_M \neq 0$).

In light of our results, the nearly degenerate d_{xz}/d_{yz} bands which are below E_F at Γ in the 2 ML film show that ferro-orbital order should not be the origin of nematic order in FeSe. Moreover, in thinner films, Δ_M is larger, Δ_Γ is smaller, and the nematic transition temperature is also higher [8,27-29]. This result indicates that the d-wave Pomeranchuk instability is the driving force of the nematic transition. Accordingly, the sign-change momentum-dependent nematic order observed in bulk FeSe is likely composed of the leading d-wave nematic order and thickness-dependent ferro-orbital order. Although one previous proposal has suggested that the three orbital orders may lead to accidental degeneracy [30], this hypothesis can be ruled out by the temperature-dependent measurement because different orbital orders should have a different temperature dependence (see Fig. S2 in Supplementary Materials). For the microscopic origin of Pomeranchuk instability observed here, one possibility is the interatomic Coulomb repulsion that induces the d-wave bond nematic order owing to the van Hove singularity at M close to the Fermi level [8], which is consistent with our results. It is also possible that the Pomeranchuk instability is driven by the spin fluctuation mediated Landau interaction in the $l=2$ charge sector [6,31,32], which needs to be further verified. Our results provide concrete constraints on the possible microscopic origin of nematicity order in FeSe [6].

The absence of the SOC gap also raises a question regarding the origin of the lifting of the d_{xz}/d_{yz} degeneracy at the Γ point with increasing number of layers. For iron-based superconductors, SOC has been widely observed and discussed [33-36]. SOC can induce a gap at the Γ point without breaking the rotational symmetry. Therefore, one natural possibility is that the SOC strength in the 2 ML film is largely weakened compared to the other iron-based materials. A previous ARPES study has already shown that the SOC strength is material dependent in iron-based superconductors [33]. Although the atomic SOC strength is the same, the effective SOC strength in materials largely depends on the crystal field, electron correlations [37] and possibly spin fluctuations [38-41], which are likely thickness-dependent.

Our observations show a purely d-wave Pomeranchuk nematic order in the floating monolayer FeSe by *in situ* ARPES studies. The Pomeranchuk instability induces the nematic distortion of FSs and lifts the d_{xz} and d_{yz} degeneracy around the M point, as shown in Fig. 4c. On the contrary, the d_{xz} and d_{yz} below the Fermi level are still degenerate around the Γ point, which rules out the ferro-orbital order as illustrate in Fig. 4c. Moreover, by investigating nematic 2 ML FeSe, the d-wave FS distortion and the nearly degenerate d_{xz} and d_{yz} bands at the Γ point clearly reveal that the driving force of nematic order in floating monolayer FeSe is the FS Pomeranchuk instability. Further investigating the thickness-dependent FeSe thin films, we detect that the momentum-dependent nematic order in bulk FeSe can be composed of two main parts: the leading d-wave FS distortion and the thickness-dependent ferro-orbital order. Additionally, many unconventional features of high-T_c materials, including electronic nematicity, originate from their quasi-two-dimensional nature, where quantum fluctuations are strongly enhanced. Our findings demonstrate that a two-dimensional limit system not only provides new insight into the properties of those materials, but also makes it possible to reveal the fundamental physics in the two-dimensional limit.

Methods

High-quality FeSe films for *in situ* ARPES measurements are grown on 0.7 wt% Nb-doped SrTiO$_3$ (001) substrates after degassing for 10 hours at 600 °C and then annealing for 1.5 hours at 950 °C in an ultrahigh vacuum molecular beam epitaxy (MBE) chamber. Substrates are kept at 310 °C during film growth. Fe (99.98%) and Se (99.999%) are co-evaporated from Knudsen cells. The flux ratio of Fe to Se is 1:10, which is measured by a quart crystal balance. The growth rate is determined by the Fe flux and equals 0.7 UC/min. During the growth process, the sample quality is monitored using reflection high-energy electron diffraction (RHEED). After growth, the FeSe films are annealed at 370 °C for 10 hours. Then, the samples are transferred *in situ* to the ARPES chamber for measurements. The ARPES measurements are recorded at the BL-09U "Dreamline" beamline of the Shanghai Synchrotron Radiation Facility (SSRF) using a VG DA30 electron analyser under an ultrahigh vacuum better than 5×10^{-11} torr. The energy resolution is set to ~12 meV for the band structure and ~16 meV for FS mapping, while the angular resolution is set to 0.2°. The spectra are recorded at 30 K unless otherwise indicated. The scanning tunneling microscopy (STM) measurements are conducted in an ultrahigh vacuum STM (Unisoku) with a base temperature of 4.2 K. A polycrystalline PtIr STM tip is used and calibrated on an Ag island before the STM experiments.

References

1. Keimer, B., Kivelson, S. A., Norman, M. R., Uchida, S. & Zaanen, J. From quantum matter to high-temperature superconductivity in copper oxides. *Nature* **518**, 179 (2015).

2. Wu, J., Bollinger, A., He, X. & Božović, I. Spontaneous breaking of rotational symmetry in copper oxide superconductors. *Nature* **547**, 432-435 (2017).

3. Johnston, D. C. The puzzle of high temperature superconductivity in layered iron pnictides and chalcogenides. *Adv. Phys.* **59**, 803 (2010).

4. Paglione, J. & Greene, R. L. High-temperature superconductivity in iron-based materials. *Nat. Phys.* **6**, 645-658 (2010).

5. Kuo, H. H., Chu, J. H., Palmstrom, J. C., Kivelson, S. A. & Fisher, I. R. Ubiquitous signatures of nematic quantum criticality in optimally doped Fe-based superconductors. *Science* **352**, 958-962 (2016).

6. Fernandes, R. M., Chubukov, A. V. & Schmalian, J. What drives nematic order in iron-based superconductors? *Nat. Phys.* **10**, 97 (2014).

7. Le, T. *et al.* Evidence for nematic superconductivity of topological surface states in PbTaSe$_2$. *Sci. Bull.* **65**, 1349-1355 (2020).

8. Jiang, K., Hu, J. P., Ding, H. & Wang, Z. Q. Interatomic Coulomb interaction and electron nematic bond order in FeSe. *Phys. Rev. B* **93**, 115138 (2016).

9. Lee, C. C., Yin, W. G. & Ku, W. Ferro-Orbital Order and Strong Magnetic Anisotropy in the Parent Compounds of Iron-Pnictide Superconductors. *Phys. Rev. Lett.* **103**, 267001 (2009).

10. Pomeranchuk, I. I. On the stability of a Fermi liquid. *Sov. Phys. JETP* **8**, 361 (1958).

11. Suzuki, Y. *et al.* Momentum-dependent sign inversion of orbital order in superconducting FeSe. *Phys. Rev. B* **92**, 205117 (2015).

12. Pfau, H. *et al.* Momentum Dependence of the Nematic Order Parameter in Iron-Based Superconductors. *Phys. Rev. Lett.* **123**, 066402 (2019).

13. Yi, M. *et al.* Nematic Energy Scale and the Missing Electron Pocket in FeSe. *Phys. Rev. X* **9**, 041049 (2019).

14. Huh, S. S. *et al.* Absence of Y-pocket in 1-Fe Brillouin zone and reversed orbital occupation imbalance in FeSe. *Commun. Phys.* **3**, 52 (2020).

15. Zhang, Y. *et al.* Distinctive orbital anisotropy observed in the nematic state of a FeSe thin film. *Phys. Rev. B* **94**, 115153 (2016).

16. Li, W. *et al.* Stripes developed at the strong limit of nematicity in FeSe film. *Nat. Phys.* **13**, 957 (2017).

17. Huang, D. *et al.* Bounds on nanoscale nematicity in single-layer FeSe/SrTiO₃. *Phys. Rev. B* **93**, 125129 (2016).

18. Xie, Y., Feng, J., Xiang, H. & Gong, X. Interplay of Strain and Magnetism in FeSe Monolayers. *Chin. Phys. Lett.* **36**, 056801 (2019).

19. Liu, X. *et al.* Dichotomy of the electronic structure and superconductivity between single-layer and double-layer FeSe/SrTiO₃ films. *Nat. Commun.* **5**, 5047 (2014).

20. Sutter, P. W., Flege, J.-I. & Sutter, E. A. Epitaxial graphene on ruthenium. *Nat. Mater.* **7**, 406 (2008).

21. Zhang, H. M. *et al.* Origin of charge transfer and enhanced electron-phonon coupling in single unit-cell FeSe films on SrTiO₃. *Nat. Commun.* **8**, 214 (2017).

22. Zhao, W. W. *et al.* Direct imaging of electron transfer and its influence on superconducting pairing at FeSe/SrTiO₃ interface. *Sci. Adv.* **4**, eaao2682 (2018).

23. Tan, S. Y. *et al.* Interface-induced superconductivity and strain-dependent spin density waves in FeSe/SrTiO₃ thin films. *Nat. Mater.* **12**, 634 (2013).

24. Richard, P., Qian, T. & Ding, H. ARPES measurements of the superconducting gap of Fe-based superconductors and their implications to the pairing mechanism. *J. Phys.:Condens. Matter* **27**, 293203 (2015).

25. Yeh, J. J. & Lindau, I. Atomic Subshell Photoionization Cross-Sections and Asymmetry Parameters : $1 \leqslant Z \leqslant 103$. *At. Data Nucl. Data Tables* **32**, 1-155 (1985).

26. Peng, X. L. *et al.* Observation of topological transition in high-T_c superconducting monolayer FeTe$_{1-x}$Se$_x$ films on SrTiO₃(001). *Phys. Rev. B* **100**, 155134 (2019).

27. Zhang, P. *et al.* Observation of two distinct d_{xz}/d_{yz} band splittings in FeSe. *Phys. Rev. B* **91**, 214503 (2015).

28. Su, Y. H., Liao, H. J. & Li, T. The form and origin of orbital ordering in the electronic nematic phase of iron-based superconductors. *J. Phys.:Condens. Matter* **27**, 105702 (2015).

29. Liang, Y., Wu, X. X. & Hu, J. P. Electronic Structure Properties in the Nematic Phases of FeSe. *Chin. Phys. Lett.* **32**, 117402 (2015).

30. Yu, R., Zhu, J.-X. & Si, Q. Orbital selectivity enhanced by nematic order in FeSe. *Phys. Rev. Lett.* **121**, 227003 (2018).

31. Wang, F., Kivelson, S. A. & Lee, D.-H. Nematicity and quantum paramagnetism in FeSe. *Nat. Phys.* **11**, 959-963 (2015).

32. Fanfarillo, L. *et al.* Orbital-dependent Fermi surface shrinking as a fingerprint of nematicity in FeSe. *Phys. Rev. B* **94**, 155138 (2016).

33. Borisenko, S. V. *et al.* Direct observation of spin-orbit coupling in iron-based superconductors. *Nat. Phys.* **12**, 311 (2016).

34. Johnson, P. D. *et al.* Spin-Orbit Interactions and the Nematicity Observed in the Fe-Based Superconductors. *Phys. Rev. Lett.* **114**, 167001 (2015).

35. Day, R. P. *et al.* Influence of Spin-Orbit Coupling in Iron-Based Superconductors. *Phys. Rev. Lett.* **121**, 076401 (2018).

36. Ma, M. W. *et al.* Prominent Role of Spin-Orbit Coupling in FeSe Revealed by Inelastic Neutron Scattering. *Phys. Rev. X* **7**, 021025 (2017).

37. Zhou, S., Jiang, K., Chen, H. & Wang, Z. Correlation Effects and Hidden Spin-Orbit Entangled Electronic Order in Parent and Electron-Doped Iridates Sr_2IrO_4. *Phys. Rev. X* **7**, 041018 (2017).

38. Wang, Q. S. *et al.* Magnetic ground state of FeSe. *Nat. Commun.* **7**, 12182 (2016).

39. Luo, C. W. *et al.* Unveiling the hidden nematicity and spin subsystem in FeSe. *npj Quantum Mater.* **2**, 32 (2017).

40. Wang, P. S. *et al.* Robust short-range-ordered nematicity in FeSe evidenced by high-pressure NMR. *Phys. Rev. B* **96**, 094528 (2017).

41. He, M. *et al.* Evidence for short-range magnetic order in the nematic phase of FeSe from anisotropic in-plane magnetostriction and susceptibility measurements. *Phys. Rev. B* **97**, 104107 (2018).

Acknowledgements

Author contributions

X.-L.P., Y.-H.Y., W.L. and Y.-J.S. synthesized the samples; X.-L.P. performed the ARPES measurements with help from S.-Y.G, and Y.-B.H.; X.-L.P., and Y.-J.S. analyzed the ARPES data; Y.-H.Y, W.L. and Q.-K.X performed the STM/STS measurements and analysed the data; K.J. and Z.-Q.W. provided theoretical input; X.-L.P., K.J., and Y.-J.S. wrote the manuscript; All authors discussed the results and commented on the manuscript; Y.-J.S. and H.D. supervised the project.

Competing interests

The authors declare no competing interests.

Data and materials availability

All data needed to evaluate the conclusions in the paper are present in the paper and/or the Supplementary Materials. Materials and additional data related to this paper may be requested from the authors.

Additional information

Correspondence and requests for materials should be addressed to Y.-J.S. (yjsun@iphy.ac.cn) and H.D. (dingh@iphy.ac.cn).
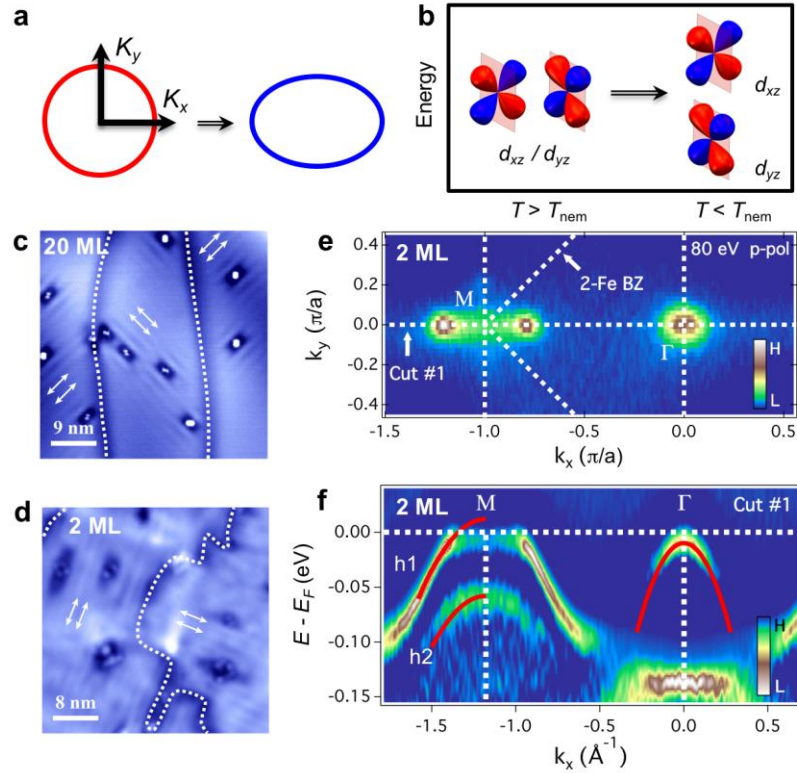
Fig. 1 | Nematicity in multilayer FeSe films on SrTiO₃ (STO). a, Schematic of Pomeranchuk instability induced Fermi surface distortion and **b,** imbalance occupation in d_{xz}/d_{yz} orbital induced Ferro-orbital order, respectively. **c,** STM topographic image of a 20 ML FeSe film on STO (45 nm × 45 nm; $V = 60$ mV, $I = 40$ pA). The white arrows indicate the stripes with twofold symmetry developed in the vicinity of impurities. The direction of stripes rotates 90° when crossing the domain walls (the white dashed lines). **d,** Same as **c** but for a 2 ML FeSe film on STO (40 nm × 40 nm; V = 60 mV, I = 100 pA). **e,** The Fermi surface of 2 ML FeSe/STO measured by 80 eV p-polarized photons at T = 20 K. The intensity has been integrated in the ±10 meV energy range. **f,** Second-derivative spectrum of the band structure of 2 ML FeSe/STO measured by 80 eV p-polarized photons along the Γ - M direction indicated by Cut #1 in **e**. The red lines represent the energy band near the Γ and M points. Bands h1 and h2 are two hole-like bands.
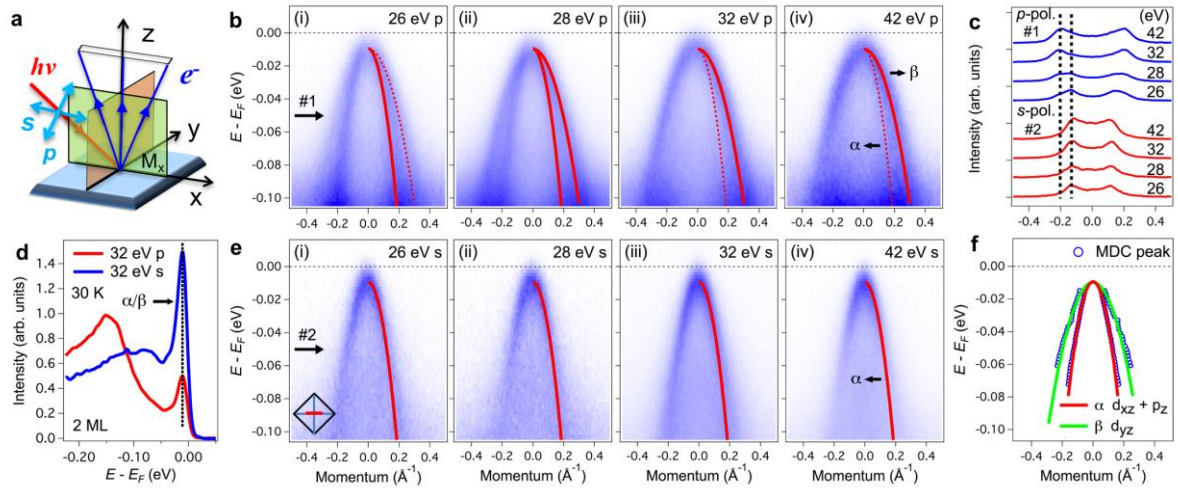
Fig. 2 | d_{xz}/d_{yz} degeneracy at the Brillouin Zone centre (Γ) in floating monolayer FeSe on FeSe/STO. a, Schematic experimental geometry of the ARPES measurements. **b,** Band structure measured by (i) 26 eV, (ii) 28 eV, (iii) 32 eV and (iv) 42 eV *p*-polarized photons along the Γ - M direction. The red lines represent the fitting results of two hole-like bands. Solid and dashed lines indicate the visible and invisible bands, respectively. **c,** Comparison of the momentum distribution curve (MDC) measured by different photon energies and polarizations at the energies indicated by #1 in **b** and #2 in **e**. The black dashed lines indicate the peak position. **d,** Comparison of the energy distribution curve (EDC) at the Γ point measured by 32 eV *p*- and *s*-polarized photons. The black dashed lines indicate the positions of the α and β band tops. **e,** Same as **b** but measured by *s*-polarized photons. **f,** Summary of the band structure and orbital analysis around Γ. Blue circles represent the peak position of MDC fitted by the Lorentz function. Two solid curves are the fitting results of MDC peaks.
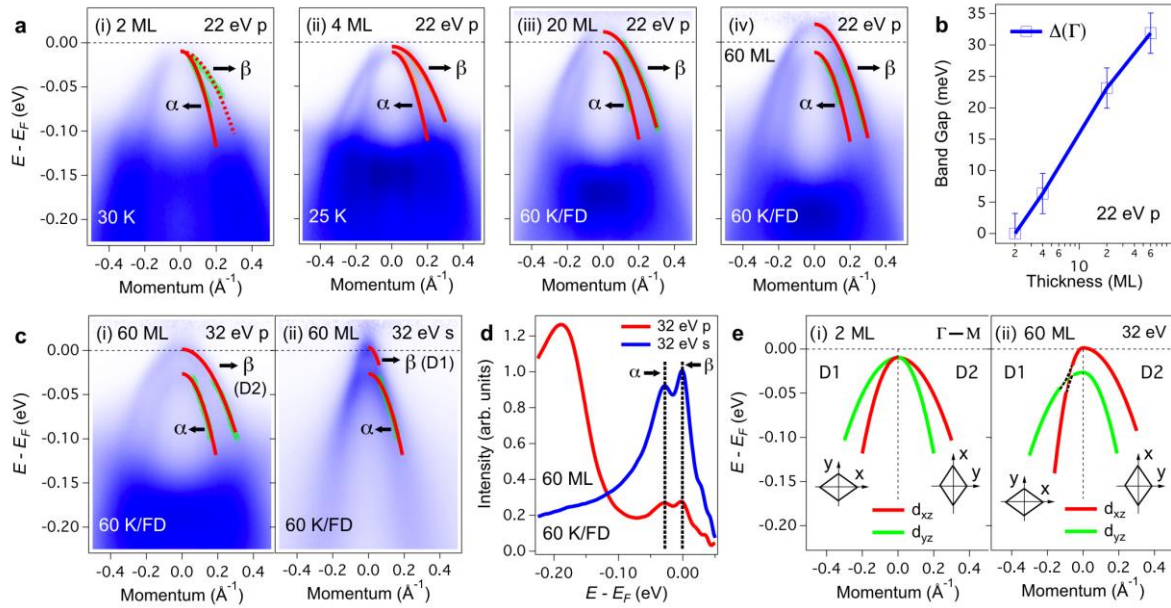
Fig. 3 | Thickness-dependent d_{xz}/d_{yz} band gap and nematic order around the Γ point. a, Band structure of (i) 2 ML, (ii) 4 ML, (iii) 20 ML and (iv) 60 ML FeSe measured by 22 eV p-polarized photons along the Γ – M direction. The results of 20 ML and 60 ML are divided by the Fermi–Dirac distribution function convoluted by the resolution function to visualize the states above E_F. Red lines represent the fitting results of band dispersion. **b,** The evolution of the band gap between α and β with film thickness. **c,** Band structure along the Γ – M direction of 60 ML FeSe measured by 32 eV (i) p- and (ii) s- polarized photons. The red lines represent the band dispersion of the α and β bands. D1 and D2 represent domain 1 and domain 2. **d,** Comparison of the energy distribution curve (EDC) at the Γ point of the data in **c**. The black dashed lines indicate the positions of the α and β band tops. **e,** Schematic band structure around the Γ point of (i) 2 ML and (ii) 60 ML for two perpendicular domains. The x-axis is defined along the longer Fe-Fe direction for both domains.
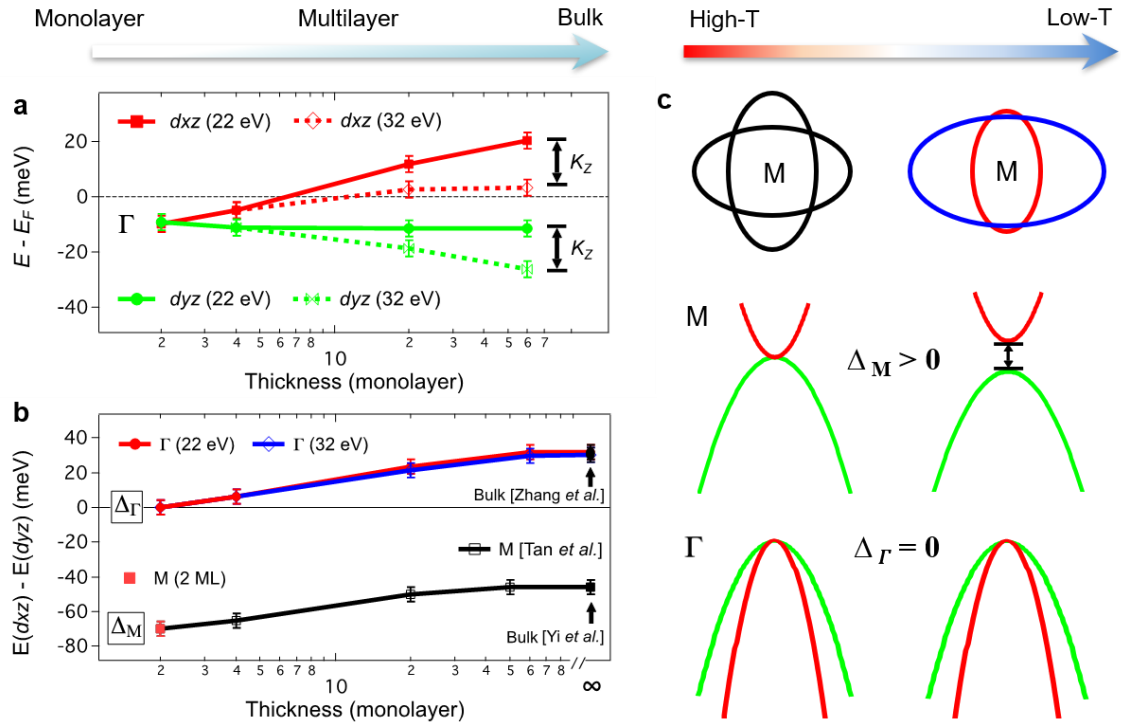
Fig. 4 | Summary of thickness-dependent nematic order in FeSe films on STO. a, Summary of the thickness-dependent binding energy of hole-like bands at the Γ point and the corresponding orbital character measured by 22 eV and 32 eV photons. k_z represents the variation of the band top with photon energy. **b,** Summary of the evolution of the onsite energy difference between the d_{xz} and d_{yz} orbitals at Γ and M point with film thickness. The data of bulk FeSe are adapted from ref. [27] for the Γ point and ref. [13] for the M point. The data of the M point of multilayer FeSe are adapted from ref. [23]. **c,** Schematic of the Pomeranchuk instability induced nematic distortion of FSs and band structure evolution near M and Γ point observed in 2 ML FeSe/STO, respectively.

Supplementary Materials

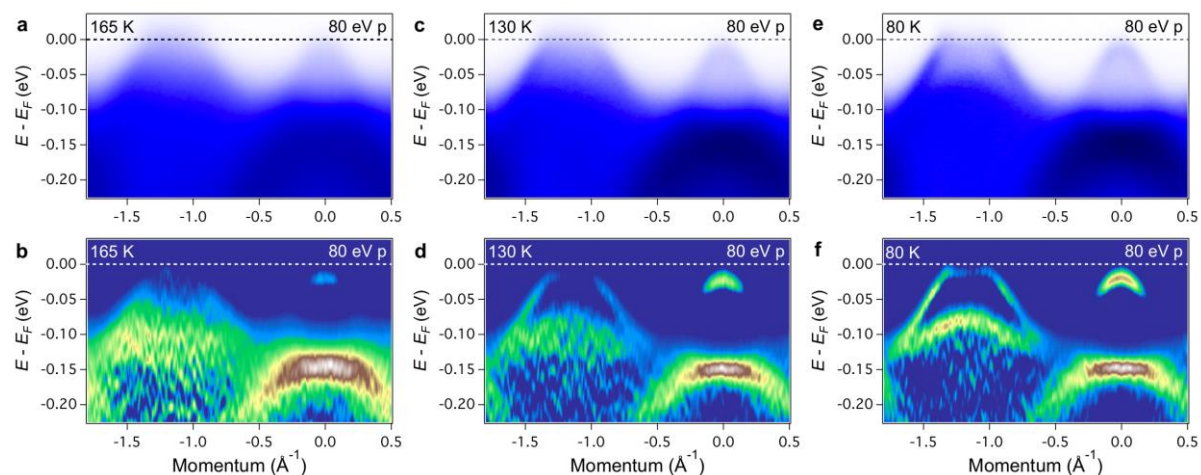**This PDF file includes:**

Figures S1 to S2

Figure S1 | Temperature dependence of nematic band splitting in 2 ML FeSe/STO. a-b, Electronic structure along Γ - M direction detected by 80 eV p-polarized photons and the corresponding second derivative spectrum. The data is measured at T = 165 K. **c-d** and **e-f** Same as **a-b** but measured at T = 130 K and 80 K, respectively. As temperature decreases, nematic band splitting at M point becomes larger. This behavior is consistent with the results observed in bulk materials and supports that the nematic order also exists in 2 ML FeSe/STO.
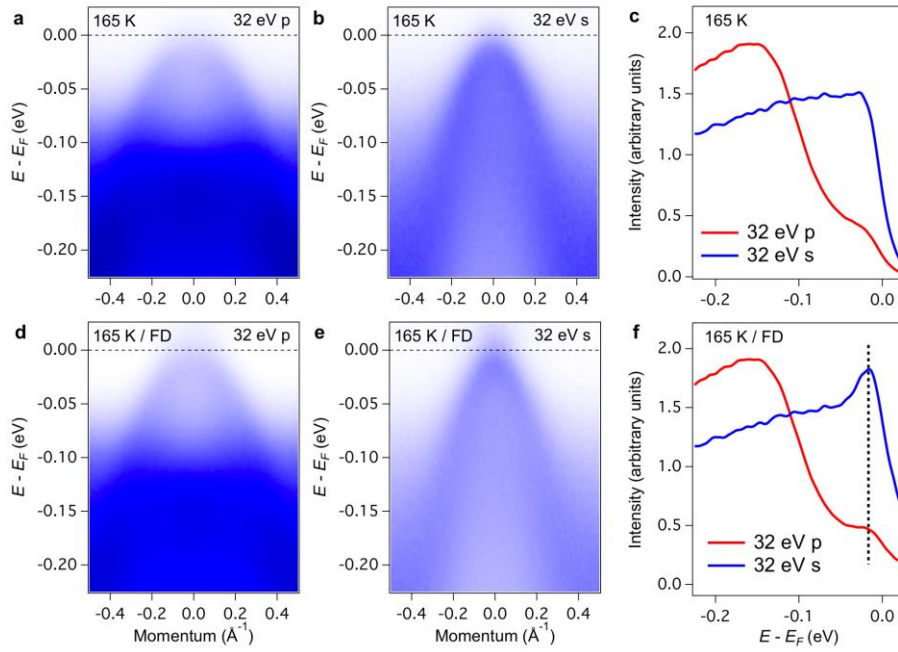
Figure S2 | Γ point d_{xz}/d_{yz} degeneracy at high temperature in 2 ML FeSe/STO. a-b, Band structure along Γ – M direction measured at T = 165 K by 32 eV *p-* and *s-* polarized photons, respectively. **c,** Comparison of energy distribution curve (EDC) at Γ point measured by 32 eV *p-* and *s-*polarized photons. **d-e,** Band structure along Γ – M direction measured at T = 165 K by 32 eV *p-* and *s-* polarized photons, respectively, which are divided by the Fermi–Dirac distribution function convoluted by the resolution function to highlight the states near and above Fermi energy. **f,** Comparison of energy distribution curve (EDC) at Γ point measured by 32 eV *p-* and *s-*polarized photons. The black dashed lines indicate the position of α and β band top.